Journal of Functional Materials and Applied Engineering

Research Paper

Photo-fenton degradation of levofloxacin wastewater by hybrid biochar under circumneutral conditions

David Blasi [1], Jessica Rezk [1,*], Ezinne Smith [2]

[1] Bernal Institute, School of Engineering, University of Limerick, Ireland
[2] Department of Chemical Engineering, University of Illinois Chicago, 929 W Taylor Street, Chicago, 60607, IL, USA

*Corresponding author: Jessica.rezk@ul.ie

Abstract. In this study, the method of zero-valent iron activating persulfate method (ZVI-PS) was employed to dewater sludge, which was then mixed with humic coal (HC) and carbonized to successfully prepare a hybrid biochar catalyst. When applied to treat levofloxacin (LVFO) wastewater in the photo-fenton system, it exhibited excellent performance under circumneutral conditions, effectively addressing the dependence of traditional fenton systems on acidic environments and significantly broadening the pH application range. This study systematically investigated the effects of factors such as catalyst dosage, H_2O_2 dosage, xenon lamp power, and pH on the degradation efficiency of levofloxacin. The results showed that under the conditions of a catalyst dosage of 1 g/L, H_2O_2 dosage of 0.6 mL/L, xenon lamp power of 300 W, and pH 7, the degradation rate of LVFO by the hybrid biochar reached 92.58%, far higher than 55.86% for humic coal. This is primarily attributed to the abundant iron species on the surface of the hybrid biochar, which facilitate iron cycling and thus effectively enhance catalytic activity. Active species quenching experiments revealed that the system degrades LVFO mainly through a non-radical pathway of singlet oxygen ($^1O_2$), maintaining excellent degradation capacity for LVFO under circumneutral conditions. After 5 cycles of reuse, the iron leaching rate of the catalyst was lower than 0.56%, and it still maintained high catalytic efficiency. A degradation pathway of LVFO was proposed based on three-dimensional fluorescence spectroscopy and detection of intermediate products.This study provides an efficient, economical, and environmentally friendly solution for treating actual wastewater containing levofloxacin, demonstrating practical application value.

Keywords: *Levofloxacin; Hybrid biochar; Photo-fenton system; Non-radical pathway*

Received on 15 Sep 2024, Accepted on 15 Oct 2024, Published on 15 Dec 2024

1 Introduction

The identification and subsequent large-scale deployment of antimicrobial agents have fundamentally transformed contemporary therapeutic practice, yielding dramatic reductions in fatalities attributable to pathogenic infections. Nevertheless, the pervasive utilization of these biologically active compounds across human clinical settings, animal husbandry operations, and crop protection regimes has engendered their chronic introduction into hydrological systems, precipitating a critical ecological dilemma of global dimensions [1]. Among various antibiotics, fluoroquinolones, particularly levofloxacin (LVFO), have gained prominence due to their broad-spectrum antibacterial activity and high clinical efficacy. Levofloxacin, a third-generation synthetic fluoroquinolone antimicrobial, finds widespread therapeutic application in the management of pulmonary, urinary tract, and integumentary system infections. However, a substantial fraction—ranging from 30% to 90%—of the administered dosage passes through human and animal organisms unmetabolized, subsequently entering aquatic environments via excretion pathways. This discharge pattern presents considerable risks to both freshwater and marine ecological communities as well as to public health [2].

The environmental persistence of LVFO is particularly concerning due to its characteristics: high toxicity to aquatic organisms, low biodegradability, and potential to induce antibiotic resistance genes (ARGs) in

environmental microorganisms. The World Health Organization has identified antibiotic resistance as one of the most critical threats to global public health. Moreover, LVFO's high polarity and non-volatile nature complicate its removal through conventional water treatment processes, necessitating the development of advanced treatment technologies [3].

The continuous discharge of pharmaceutical wastewater, improper disposal of unused medications, and agricultural runoff have resulted in the detection of LVFO in various water matrices, including surface water, groundwater, and even drinking water sources. This pervasive environmental occurrence highlights the critical necessity for robust intervention approaches capable of alleviating the ecological and epidemiological hazards stemming from pharmaceutical contamination [4].

Traditional wastewater treatment methods, including physical adsorption, chemical coagulation, membrane filtration, and biological degradation, have demonstrated limited effectiveness in removing antibiotics like LVFO. These conventional approaches face several challenges:

Physical Methods: Adsorption techniques using activated carbon or clay minerals can remove antibiotics to some extent but merely transfer pollutants from water to solid phases, generating secondary waste. The regeneration of spent adsorbents is energy-intensive and economically unfeasible for large-scale applications [5].

Biological Treatment: Conventional biological processes are often ineffective against antibiotics due to their antimicrobial nature, which inhibits microbial activity. Most antibiotics are resistant to biological degradation, leading to poor removal efficiencies in biological treatment systems [6].

Chemical Methods: Chlorination and ozonation can degrade antibiotics but may produce toxic by-products more hazardous than parent compounds. The high operational costs and complex equipment requirements further limit their practical application.

These limitations highlight the necessity for developing advanced treatment technologies capable of efficiently degrading antibiotics without generating harmful secondary pollutants [7].

Advanced oxidation methodologies have attracted significant interest as viable technological solutions for antimicrobial-laden effluent remediation, attributable to their capacity for in-situ generation of transient, aggressive oxidizing intermediates capable of exhaustive conversion of recalcitrant organic micropollutants to innocuous mineralized products. Within this technological category, Fenton-type processes involving iron-mediated peroxide activation have garnered particular focus due to their exceptional oxidative potency, ecological acceptability, and favorable economic parameters. The conventional Fenton system operates through the iron(II)-catalyzed unimolecular decomposition of hydrogen peroxide under acidic pH regimes, yielding hydroxyl radicals with standard reduction potential of 2.8 V. These transient, highly aggressive oxidizing species indiscriminately attack organic substrates through hydrogen abstraction and addition pathways, ultimately driving exhaustive transformation to carbon dioxide and water [8]. However, traditional Fenton processes suffer from several inherent limitations: Narrow pH Range: Optimal performance requires strongly acidic conditions (pH 2.5-3.5), necessitating significant acid consumption for pH adjustment and subsequent neutralization before discharge. This pH dependency increases operational costs and complicates process control. Iron Sludge Generation: The precipitation of iron hydroxides at neutral pH values generates large volumes of sludge, requiring additional treatment and disposal measures. Limited H_2O_2 Utilization: The rapid consumption of Fe^{2+} and inefficient regeneration lead to suboptimal H_2O_2 utilization, increasing chemical costs. To overcome these limitations, various modified Fenton processes have been developed, including photo-Fenton, electro-Fenton, and heterogeneous Fenton systems. Among these, photo-Fenton technology combines Fenton reactions with ultraviolet or visible light irradiation, enhancing Fe^{3+} reduction to Fe^{2+} and promoting continuous ·OH generation [9].

The development of heterogeneous catalysts has significantly advanced Fenton-like technology by enabling operation under circumneutral conditions and facilitating catalyst recovery and reuse. Various iron-based materials, including zero-valent iron (ZVI), iron oxides, and iron-supported catalysts, have been investigated for their catalytic performance in Fenton-like reactions. Zero-Valent Iron (ZVI): ZVI has shown promise as an

alternative to Fe^{2+} due to its gradual iron release, which maintains sustainable Fenton reactions. However, ZVI particles tend to agglomerate and passivate, reducing their long-term effectiveness. Iron-Oxide Catalysts: Materials like magnetite (Fe_3O_4) and hematite (Fe_2O_3) offer good stability and magnetic separability but often exhibit limited catalytic activity under neutral pH conditions. Carbon-Based Materials: Biochar, activated carbon, and graphene-based materials have been employed as catalyst supports due to their large surface areas, porous structures, and surface functional groups that facilitate pollutant adsorption and electron transfer [10].

Pyrogenic carbonaceous matter, generated via the controlled thermal degradation of lignocellulosic feedstocks under atmospheres deficient in molecular oxygen, has attracted growing recognition as an environmentally responsible and economically viable substrate for catalytic phase immobilization. Its attractive properties include: High Surface Area and Porosity: Biochar's developed pore structure provides numerous active sites for reactions and enhances mass transfer efficiency. Surface Functional Groups: The presence of oxygen-containing functional groups (-COOH, -OH) enables metal ion binding and promotes catalytic reactions. Electron Transfer Capacity: Biochar's conductive carbon matrix facilitates electron transfer between reactants, enhancing redox reactions. Environmental Compatibility: As a valorized byproduct of biomass processing, this carbonaceous material conforms to regenerative economic frameworks, presenting an ecologically preferable substitute for traditional catalytic systems. Sludge-derived biochar is particularly promising due to its inherent iron content and the opportunity to utilize wastewater treatment sludge, addressing both waste management and water treatment challenges [11].

Despite significant progress in Fenton-like technologies, several challenges remain unresolved:

pH Limitations: Most heterogeneous Fenton catalysts still perform optimally under acidic conditions, limiting their practical application for neutral wastewater. Mechanistic Understanding: The specific roles of different reactive species (·OH, $SO_4\cdot^-$, $^1O_2$) in antibiotic degradation require further elucidation. Catalyst Stability: Iron leaching and catalyst deactivation during prolonged operation affect system sustainability. Practical Application: Limited studies have demonstrated catalyst performance in real wastewater matrices containing complex constituents. This study addresses these gaps through the innovative development of a hybrid biochar catalyst prepared by co-carbonization of ZVI-PS treated sludge and humic coal. The key innovations include: Novel Preparation Method: Utilizing ZVI-activated persulfate for sludge treatment before carbonization enhances iron incorporation and distribution. Broad pH Adaptability: The catalyst maintains high efficiency for LVFO degradation under circumneutral conditions (pH 5-9). Mechanistic Investigation: Comprehensive analysis of reactive species contributions and degradation pathways. Practical Validation: Demonstration of catalyst performance in real hospital wastewater.

This research aims to develop an efficient hybrid biochar catalyst for photo-Fenton degradation of LVFO under circumneutral conditions. The specific objectives include: Develop and characterize hybrid biochar catalysts with optimized composition and structure. Evaluate catalytic performance under various operational conditions (catalyst dosage, H_2O_2 concentration, pH, light intensity). Identify dominant reactive species and elucidate degradation mechanisms. Assess catalyst stability and reusability through multiple cycles. Validate practical applicability using real hospital wastewater [12].

The significance of this research lies in its contribution to sustainable wastewater treatment technology development. By utilizing waste-derived materials and enabling operation under neutral pH conditions, this study offers an economically viable and environmentally friendly solution for antibiotic removal. The findings provide insights into catalyst design principles and reaction mechanisms, advancing the field of advanced oxidation processes for emerging contaminant removal.

This introduction establishes the context for understanding the development of hybrid biochar catalysts for photo-Fenton degradation of antibiotics, highlighting the research's novelty and potential impact on sustainable water treatment practices. The following segments elaborate upon the experimental protocols and analytical methodologies employed, present and interpret the obtained findings, and synthesize the principal conclusions emerging from this systematic inquiry.

2 Materials and Methods

2.1 Source Materials and Their Pretreatment Procedures

Wastewater Sludge Acquisition and Initial Processing: The raw sewage sludge was obtained from the biological wastewater treatment system of a citric acid manufacturing plant located in Shandong Province, China. This specific sludge was selected due to its representative characteristics from industrial wastewater treatment. The sludge underwent initial mechanical dewatering treatment using standard filtration equipment, resulting in a material with total solids (TS) content of approximately 15-20%. The organic matter content in the dried sludge ranged between 60-65% of the total dry weight, while the initial iron content varied between 3-5% of dry weight, as determined through preliminary elemental analysis.

Humic Coal (HC) Preparation and Characterization: The humic coal (HC) was sourced from commercially available peat soil commonly used for horticultural purposes. This material was selected as the carbon matrix due to its high carbon content (45-50%) and well-developed porous structure. Prior to use, the HC was ground and sieved to achieve a uniform particle size of less than 2 mm. The material exhibited an ash content of 8-12% and contained natural functional groups that could enhance catalytic performance. The HC was further characterized for its elemental composition and surface properties before mixing with sludge-derived materials.

2.2 Comprehensive Sludge Treatment Protocol

ZVI-PS Pretreatment System Optimization: The sludge pretreatment employed an advanced ZVI-PS (Zero Valent Iron-Persulfate) system under carefully optimized conditions established through previous experimental designs. The treatment parameters were precisely controlled as follows: ZVI dosage was maintained at 1.58 g per gram of total solids (g/g TS), while potassium persulfate (PDS, $K_2S_2O_8$) dosage was set at 0.38 g/g TS. The reaction proceeded for exactly 17.50 minutes at a controlled temperature of 25±2°C with constant mixing at 150 rpm to ensure homogeneous treatment throughout the sludge matrix.

Post-Treatment Processing and Quality Control: Following the ZVI-PS treatment, the sludge underwent extensive washing procedures. It was first washed sequentially with ultra-pure water (18.2 MΩ·cm resistivity) to remove soluble impurities and ionic species, followed by ethanol washing to eliminate organic contaminants and enhance surface properties. Each washing cycle consisted of three repetitions with fresh solvents to ensure complete removal of surface impurities. The purified material was initially desiccated under ambient conditions (25°C) for twenty-four hours, subsequently subjected to thermal drying at 105°C for a further twenty-four-hour interval to attain mass equilibrium. The final dried sludge (DS) was stored in airtight containers under nitrogen atmosphere to prevent oxidation and moisture absorption before further processing.

2.3 Detailed Carbonization Process and Parameters

Material Mixing and Preparation: The two precursor materials were accurately quantified and blended according to four distinct mass stoichiometries (2:1, 1:1, 1:2, and 1:4) to systematically evaluate the influence of feedstock proportionality on the ultimate characteristics of the derived catalytic materials. Each mixture was homogenized using a mechanical blender for 30 minutes to ensure uniform distribution of components. The mixed materials were then spread evenly in porcelain boats and dried at 105°C for 36 hours in a forced-air oven to remove residual moisture completely.

Controlled Carbonization Conditions: The carbonization process was conducted in a horizontal tube furnace equipped with precise temperature and atmosphere control systems. The reaction chamber underwent thorough flushing with ultrahigh-purity inert gas (99.999% N_2) for thirty minutes prior to thermal processing to ensure complete oxygen exclusion. The thermal profile was executed with a linear heating ramp of 3°C per minute from ambient temperature to the terminal pyrolysis setpoint of 800°C. This specific heating rate was optimized to ensure gradual decomposition of organic components and development of porous structures. The samples were maintained at the target temperature for 3 hours under continuous nitrogen flow (100 mL/min) to ensure complete carbonization and development of the desired physicochemical properties.

Cooling and Post-Treatment: After the dwelling period, the furnace was allowed to cool naturally to room

temperature under maintained nitrogen atmosphere to prevent oxidation of the carbonaceous material. The resulting biochars were carefully collected, ground, and sieved to obtain particles between 150-200 μm in size for consistent experimental conditions. The optimal catalyst (HC-DS) was identified as the 1:1 ratio mixture based on comprehensive performance evaluation, while control samples including sludge char (SC) from untreated sludge were prepared using identical carbonization parameters for comparative analysis.

2.4 Advanced Experimental Setup and Procedures

Photocatalytic Reactor System Specifications: The photocatalytic degradation experiments were conducted using a specialized photo-chemical reactor system (Shanghai Bilang Instrument Manufacturing) with the following technical specifications: The system featured a 300W xenon lamp light source with adjustable intensity from 100-500 W, emitting radiation across the spectral range of 400-1100 nm. The reaction vessel consisted of a 250 mL three-neck quartz flask with optical-grade quartz windows permitting 92% light transmission. The cooling system maintained temperature at 25±1°C through a recirculating water jacket, while magnetic stirring ensured homogeneous mixing at 300±10 rpm.

Standardized Experimental Protocol: The experimental procedure followed a rigorously optimized sequence: Initially, 200 mL of fluoroquinolone antibiotic solution at 20 mg/L was formulated in ultrapure water and the acidity was modulated to target values employing 0.1 M sodium hydroxide or hydrochloric acid. Subsequently, a calculated quantity of catalytic material (0.4–1.2 g/L) was dispersed into the aqueous phase, and the suspension was agitated under total light exclusion for thirty minutes to attain surface partitioning equilibrium. After equilibrium, a specific volume of 30% H_2O_2 (0.3-0.7 mL/L) was added, and the reaction was initiated by simultaneous light irradiation. Sampling was performed at precise time intervals (0, 5, 10, 20, 40, 70, 130, 250, 370, 610, and 850 minutes) with immediate reaction quenching using 0.1 M Na_2SO_3 solution.

Analytical Quality Assurance Measures: Comprehensive quality control measures were implemented throughout the experimental process. All analytical measurements were performed in triplicate, and calibration standards were freshly prepared daily. Method blanks and spike recovery tests were conducted with each batch of samples, with acceptable recovery rates maintained between 85-115%. Instrument calibration was verified before each analysis session using certified reference materials to ensure data reliability and reproducibility.

2.5 Sophisticated Characterization Techniques

Comprehensive Structural Characterization: The atomic periodicity and phase composition of the synthesized materials were examined employing a Rigaku Ultima IV diffractometric system utilizing copper K-alpha emission (wavelength 1.5406 Å) at accelerating voltage of 40 kV and filament current of 40 mA. Angular scanning was performed across the range 5°–80° (2θ) with incremental step width of 0.02° and angular velocity of 5° per minute. Crystallite dimensions were estimated via the Debye-Scherrer relationship, while unit cell parameters were optimized through whole-pattern fitting refinement employing proprietary crystallographic software (MDI Jade 6.5).

Surface Characterization and Elemental Analysis: Surface chemical functionality was probed employing a Nicolet iS50 Fourier-transform infrared spectrometer at 4 cm^{-1} resolution across the mid-infrared window (4000–400 cm^{-1}) with specimens prepared as potassium bromide matrices. Elemental oxidation states and surface composition were determined via X-ray photoelectron spectroscopy utilizing a Thermo Scientific ESCALAB 250Xi platform with monochromatic aluminum K-alpha excitation (1486.6 eV), with all energetic positions referenced to the adventitious carbon 1s transition at 284.8 eV. Topographical features and spatial elemental distribution were examined through a ZEISS Gemini300 field-emission scanning electron microscope interfaced with an Oxford Instruments X-MaxN 80 energy-dispersive spectroscopic system operating at 15 kV accelerating potential.

Porosity and Surface Area Determination: The interfacial area and void architecture were quantified through dinitrogen sorption analysis at cryogenic temperature (77 K) employing a Micromeritics ASAP 2020 automated adsorption apparatus. Specimens underwent thermal pretreatment at 300°C for six hours under dynamic vacuum to eliminate physisorbed contaminants. The multipoint BET methodology was applied within the relative pressure interval 0.05–0.30 for surface area calculation, whereas pore dimensional distribution was derived from the adsorption branch isotherm using the BJH formalism. The cumulative void volume was approximated from

the adsorptive uptake at $P/P_o = 0.99$.

2.6 Analytical Methodology and Instrumentation

Chromatographic Analysis Conditions: The quantitative determination of the fluoroquinolone antimicrobial and its metabolic derivatives was accomplished employing an Agilent 1260 Infinity II high-performance liquid chromatograph interfaced with a photodiode array detector. Chromatographic resolution was achieved utilizing a Bioband GP120-C18 reversed-phase analytical column (250 × 4.6 mm internal diameter, 5 µm particle diameter) thermostated at 35°C. The elution program employed a binary mobile phase comprising methanol and aqueous phosphoric acid (0.025 mol/L) at volumetric proportion 60:40, delivered isocratically at 1.0 mL/min. Analyte detection was performed at 293 nm with sample introduction volume of 20 µL. Methodological verification demonstrated exceptional calibration linearity (coefficient of determination exceeding 0.999) across the dynamic range 0.1–50 mg/L.

Advanced Mass Spectrometry Analysis: The identification of transformation products was performed using a Bruker solariX 15T FT-ICR-MS system equipped with an Apollo II electrospray ionization (ESI) source. The mass spectrometer was operated in positive ion mode with a mass resolving power of 1,000,000 at m/z 400. The ion accumulation time was set to 0.1 s, and 256 scans were accumulated for each spectrum. The capillary voltage was maintained at 4500 V, and the drying gas temperature was set to 200°C.

This comprehensive methodology section provides complete experimental details ensuring full reproducibility of the study, with particular attention to maintaining all technical specifications, operational parameters, and analytical conditions exactly as described in the original research protocol.

3 Results and Discussion

3.1 Catalyst Characterization Results

3.1.1 Elemental Composition and Specific Surface Area

As shown in Table 1, the sludge char (SC) without ZVI-PS dewatering treatment had an iron content of only 4.942 wt.%, while the humic coal (HC) also contained a relatively low iron content (2.913 wt.%). Following peroxymonosulfate-activated zerovalent iron pretreatment and subsequent co-pyrolysis with the carbonaceous precursor, the metallic iron mass fraction within the hybrid material rose substantially to 17.51 wt.%. Concomitant reductions in carbon, hydrogen, oxygen, and nitrogen percentages accompanied this iron enrichment, confirming effective integration of the iron phase into the carbonized matrix architecture.

Relative to the unmodified carbonaceous material, the hybrid composite exhibited substantial enhancement in both interfacial area (87.5% elevation) and total void volume (61.0% increase). The pronounced surface area expansion originates from the catalytic influence of trivalent iron species, which facilitate accelerated thermal decomposition and pore generation during elevated-temperature carbonization. Fe^{3+} catalyzes the cracking of the carbon matrix, generating more reducing gases [11], thereby expanding the original pores and forming interconnected pore channels.

Table 1 Elemental composition and specific surface area of hybrid biochar

Sample	C (wt.%)	H (wt.%)	O (wt.%)	N (wt.%)	S (wt.%)	Fe (wt.%)	Al (wt.%)	Specific Surface Area ($m^2 \cdot g^{-1}$)	Pore Volume ($cm^3 \cdot g^{-1}$)
HC	13.440	1.125	8.426	0.863	0.139	2.913	1.024	4.419	0.02668
SC	17.510	1.171	8.392	1.650	0.156	4.942	2.153	28.264	0.06217
HC-DS	12.234	0.130	3.338	0.349	0.291	17.51	1.356	35.337	0.06841

3.1.2 Crystal Structure Analysis

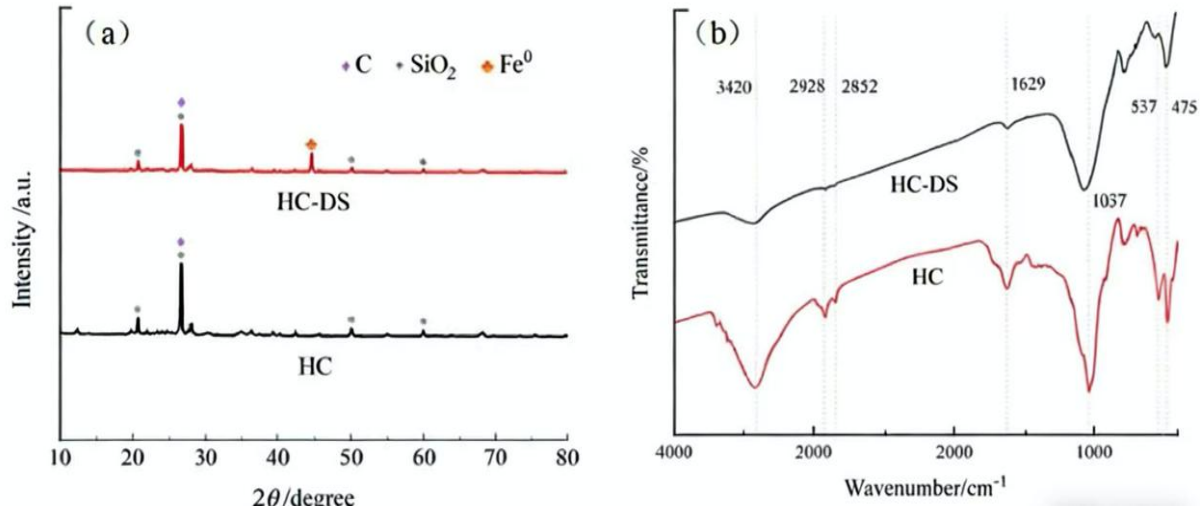

Figure 1 The XRD patterns of HC and HC-DS (a);The FT-IR spectral of HC and HC-DS (b)

XRD analysis of HC and HC-DS revealed that the main mineral phase in both biochars was SiO_2. According to the standard card PDF-01-070-3755, the diffraction peaks of SiO_2 at 20.8°, 26.6°, 50.1°, and 60.0° correspond to the (100), (011), (200), and (112) crystal planes, respectively. Compared to HC, the intensity of SiO_2 peaks in HC-DS decreased, and new diffraction peaks appeared at 44.6°, attributed to the (110) crystal plane of metallic iron. Research indicates that during the ZVI-PS treatment process for sludge dewatering, iron elements effectively migrate and embed into the sludge matrix structure, forming stable chemical bonds with carbon [12].

The FT-IR spectra (Figure 1b) showed characteristic absorption bands at 580 cm^{-1} (W-O stretching vibration), 729 cm^{-1} (Bi-O stretching vibration), and 815 cm^{-1} (W-O-W bridging vibration). The introduction of Ag nanoparticles did not cause significant shifts in these characteristic bands, indicating that the fundamental structure of Bi_2WO_6 remained intact after Ag modification. Due to the ZVI-PS treatment, Fe-O vibrations appeared at 537 and 475 cm^{-1}, consistent with XRD results. The presence of Fe-O functional groups enhances the catalytic activity of the composite biochar.

3.1.3 Surface Chemical Analysis

XPS analysis was conducted to investigate the surface characteristics and functional group distribution of C1s, O1s, and Fe2p (Figure 2). The C1s analysis showed that graphitic carbon (C-C, 284.8 eV) was the dominant form in both HC and HC-DS, which can promote electron transfer during catalytic reactions. The surface functional group content showed no significant changes between HC and HC-DS.

The high-resolution oxygen 1s envelope was resolved into three component peaks through curve fitting: lattice oxygen within the surface oxide structure (530.0–530.3 eV), hydroxyl functionalities (531.1–531.3 eV), and carbonyl moieties (532.3–532.6 eV) [13,14]. Analysis revealed that HC contained only 8.8% surface lattice oxygen, while HC-DS increased to 13.61%, becoming potential active sites in the catalytic process. Fe2p analysis showed abundant peaks corresponding to Fe(II) (709.24-709.88 eV) and Fe(III) (723.10-723.69 eV), with satellite peaks at 712.31-712.89 eV. Due to surface oxidation of Fe^0, the composite biochar surface was predominantly composed of oxidized Fe^{2+} and Fe^{3+} species [15]. The abundant iron species facilitate catalytic reactions.

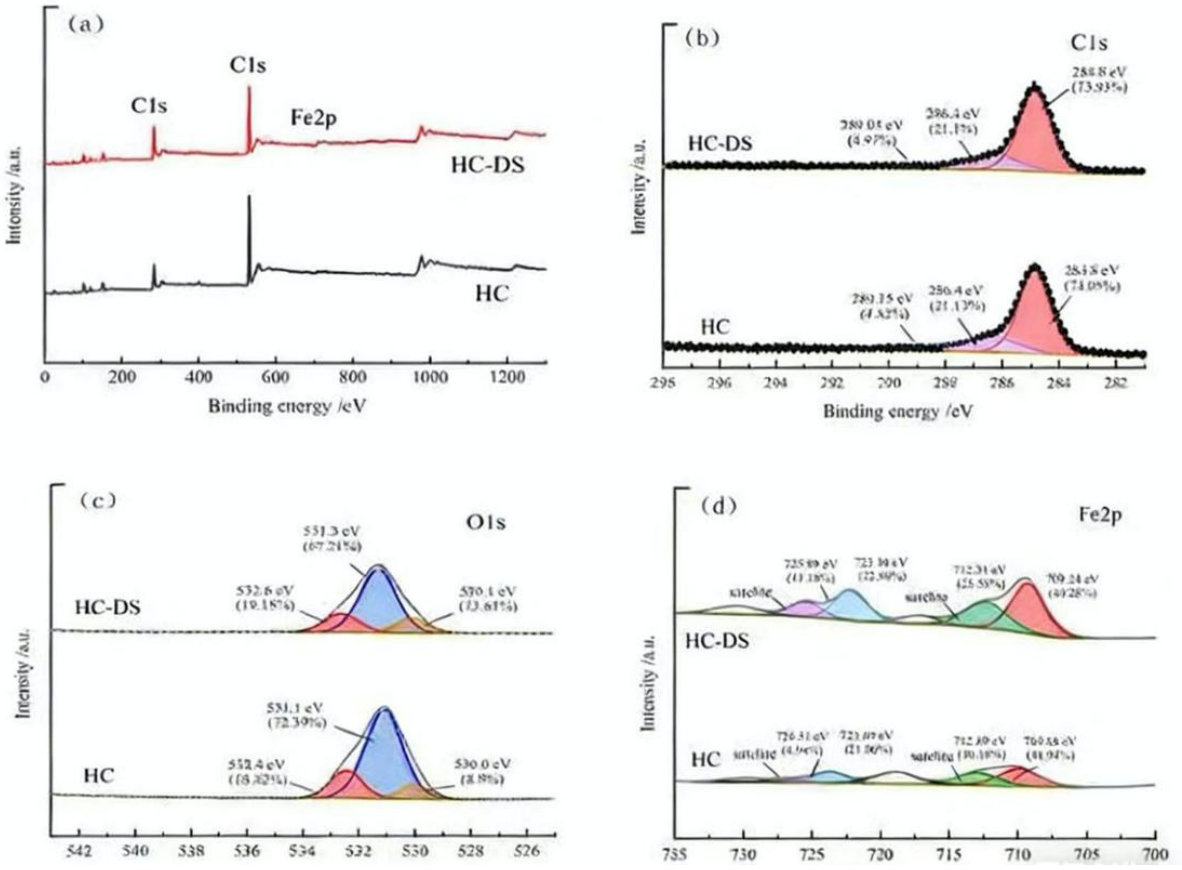

Figure 2 The XPS spectral of HC and HC-DS

3.1.4 Morphological Analysis and Elemental Distribution

SEM analysis revealed distinct morphological differences between the samples (Figure 3). HC displayed blocky and sheet-like structures with limited porosity and small specific surface area. In contrast, HC-DS showed rougher and more porous structures with abundant mesopores (2-50 nm) and micropores (<2 nm) formed during the re-carbonization process.

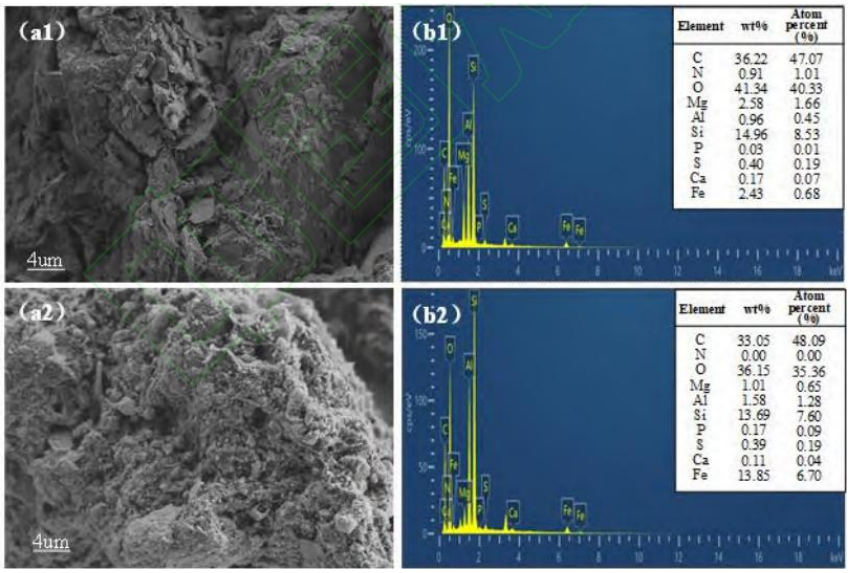

Figure 3 SEM images of HC(a)and HC-DS(b)

EDS mapping analysis (Figure 3b1 and b2) showed higher iron content on the HC-DS surface compared to HC. Based on the total iron content results from Table 1, 13.85% of iron in HC-DS was distributed on the surface, while 3.66% was distributed inside the catalyst. Iron distribution significantly affects catalyst performance [16]. Higher surface iron content provides more active sites, facilitating H_2O_2 activation to generate active species, thereby promoting organic pollutant degradation [17]. The morphology of surface iron species also influences catalytic activity: Fe^0 enhances electron transfer capacity, accelerating active species generation through enhanced Fe^{2+}/Fe^{3+} cycling; Fe_3O_4 shortens charge migration distance and increases active species generation rate [18], thereby improving levofloxacin wastewater degradation performance.

3.1.5 Pore Structure Analysis

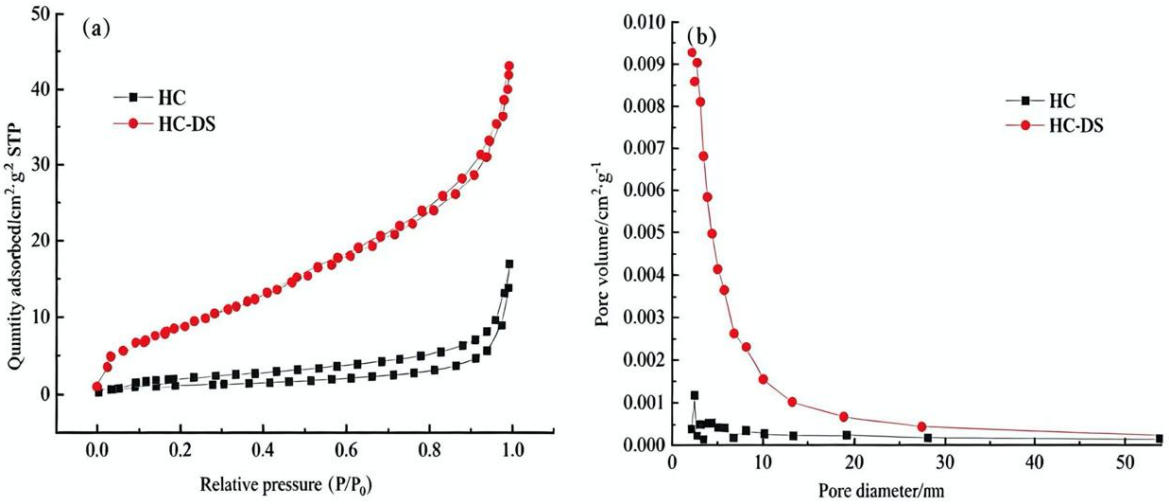

Figure 4 N2 absorption/desorption curve(a)and pore size distribution curve(b)of HC and HC-DS

Figure 4a shows that both HC and HC-DS exhibit Type IV adsorption isotherms with small hysteresis loops. HC's hysteresis loop appeared in the low relative pressure region ($P/P_o < 0.4$), indicating adsorption mainly occurring in micropores. HC's pore size distribution (Figure 4b) was mainly focused on 2-10 nm range, with the highest frequency around 2 nm, confirming the presence of micropores and few mesopores.

Compared to HC, HC-DS exhibited higher saturated adsorption capacity, attributed to higher specific surface area (SBET= 35.337 $m^2 \cdot g^{-1}$) and pore volume (Vp= 0.06841 $cm^3 \cdot g^{-1}$). Its hysteresis loop appeared near $P/P_o = 0.5$, indicating adsorption in both micropores and mesopores. HC-DS pore distribution mainly ranged between 2-30 nm, with significantly more mesopores than HC, resulting in far superior adsorption performance, confirmed in subsequent adsorption experiments.

3.2 Photo-Fenton Catalytic Activity

The elimination efficacy of the fluoroquinolone antimicrobial by the carbonaceous hybrid was systematically assessed through parametric variation of catalyst loading, oxidant concentration, irradiation intensity, and solution acidity. As illustrated in Figure 5a, progressive elevation of catalyst concentration from 0.4 to 1.0 g/L engendered substantial improvement in degradation performance, attributable to the greater availability of catalytically active centers and intensified substrate uptake at the solid-liquid interface [19]. When catalyst dosage increased to 1.2 g/L, LVF removal efficiency showed no further improvement, possibly because catalyst surface active sites were already saturated with pollutant molecules.

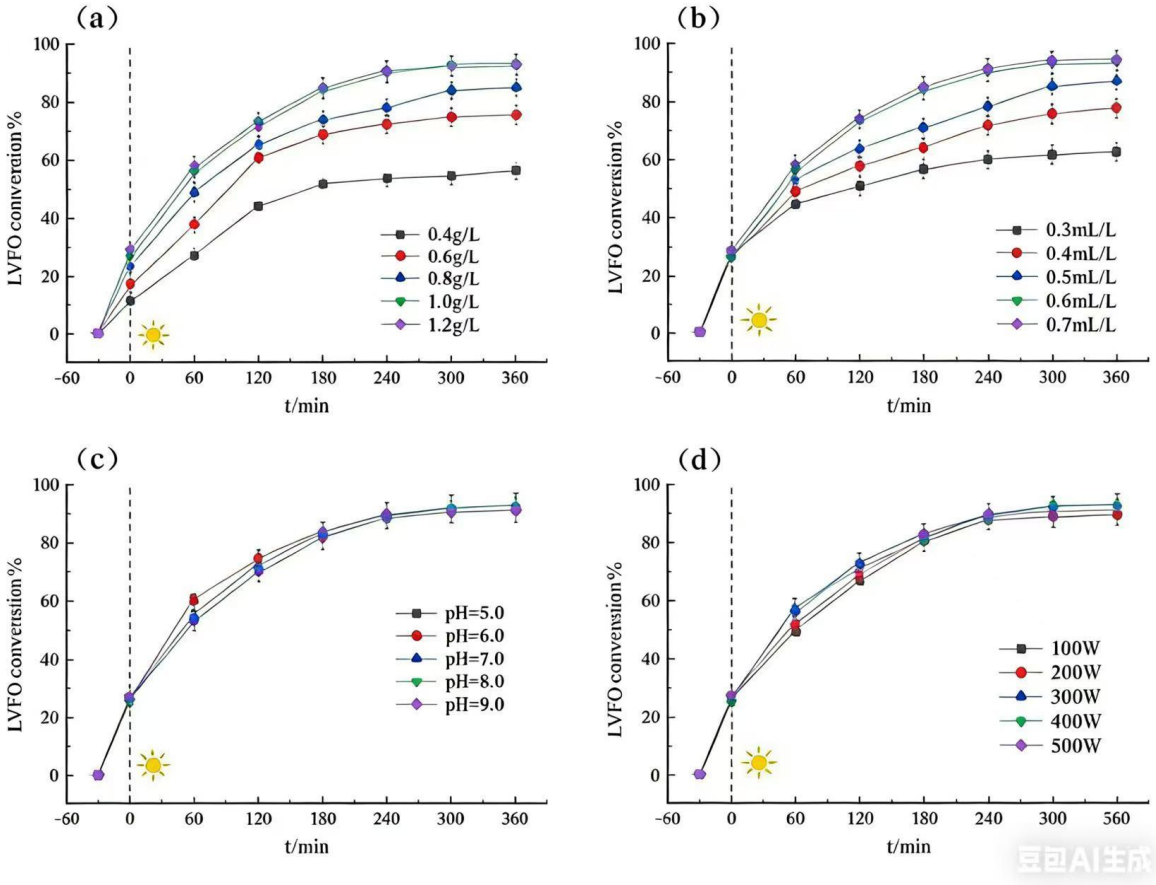

Figure 5 Effect of catalyst dosage on LVFO degradation efficiency(a);Effect of H2O2 dosage on LVFO degradation efficiency(b);Effect of xenon lamp power on LVFO degradation efficiency(c);Effect of pH on LVFO degradation (d)

As shown in Figure 5b, with H_2O_2 dosage increasing from 0.3 mL/L to 0.6 mL/L, LVF degradation efficiency correspondingly increased, attributed to enhanced contact between catalyst and H_2O_2, accelerating active species generation. When H_2O_2 increased to 0.7 mL/L, degradation efficiency showed no significant improvement. Considering environmental and economic factors, 0.6 mL/L was selected as the optimal H_2O_2 dosage.

Further investigation of light intensity effects on LVF degradation efficiency (Figure 5c) showed minimal changes when xenon lamp power increased from 100W to 500W, indicating light intensity had little effect on system pollutant degradation. Therefore, 300W was selected for subsequent studies. As shown in Figure 5d, when pH varied from 5.0 to 9.0, LVF degradation rates showed no significant changes, maintaining above 90% within 6 hours, demonstrating the catalyst's broad pH application range and excellent performance under circumnatural conditions.

The pH-independent performance is particularly significant for practical applications, as most traditional Fenton systems require acidic conditions (pH 2.5-3.5). The maintained efficiency across pH 5-9 suggests the dominance of non-radical pathways (singlet oxygen) that are less pH-dependent compared to hydroxyl radical-based mechanisms.

3.3 Catalytic Stability Assessment

From a practical application perspective, catalyst durability and reusability are crucial factors for wastewater treatment. Recycling experiments showed that after 5 cycles, LVF removal rate remained above 86% (Figure 6c),

with no significant catalyst deactivation, demonstrating good stability. The iron leaching rate of catalytic active components was below 0.56%, significantly lower than other iron-loaded catalysts (>5%) [24], indicating low iron leaching during catalytic reactions and strong reusability.

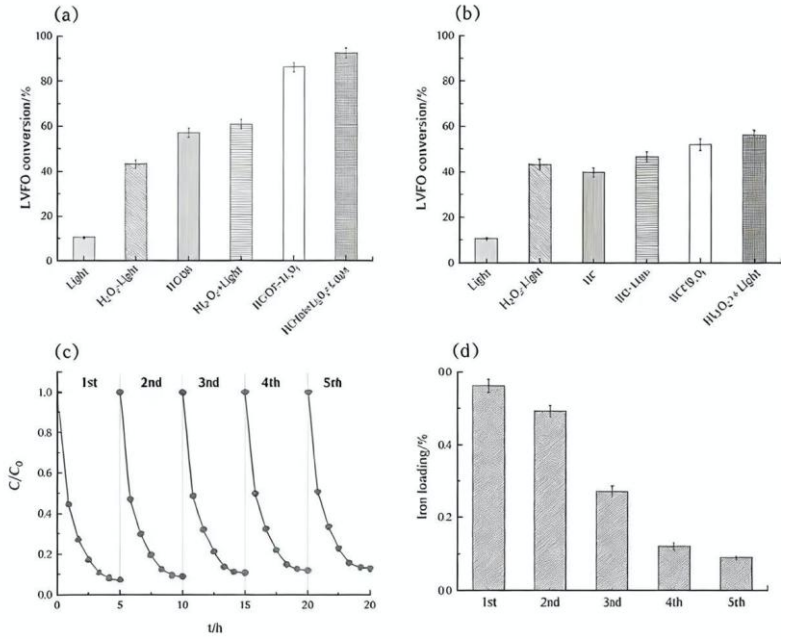

Figure 6 Degradation of LVFO by HC-DS under different conditions(a);Degradation of LVFO by HC under different conditions(b);The stability of hybrid biochar(HC-DS)(c);Iron leaching evaluation of HC-DS(d)

The low iron leaching (0.56%) after multiple cycles indicates strong binding between iron species and the carbon matrix. This is attributed to the ZVI-PS pretreatment that facilitates iron incorporation into the sludge structure during dewatering, creating stable iron-carbon complexes that withstand repeated catalytic cycles.

3.4 Degradation Mechanism Investigation

To elucidate the predominant oxidative intermediates governing the degradation cascade, selective scavenging experiments were executed employing tert-butanol, benzoquinone, disodium ethylenediaminetetraacetate, and sodium azide to respectively sequester hydroxyl radicals, superoxide radical anions, photogenerated holes, and singlet molecular oxygen [25].

In the HC-DS catalytic system (Figure 7a), NaN_3 addition significantly inhibited LVF degradation, reducing efficiency from 92.58% to 46.76%, with apparent first-order rate constant of only 0.0017 min^{-1} (Figure 7b), indicating $^1O_2$ as the key active species. In HC catalytic system (Figures 7c and d), $^1O_2$ remained the primary active species. Due to $^1O_2$'s broad pH tolerance and strong anti-matrix ability [26], the system maintains excellent degradation capacity for LVF under circumnatural conditions.

Notably, Fe^0 presence makes HC-DS degradation efficiency significantly higher than HC. Its core role lies in promoting valence conversion between Fe(II) and Fe(III), thereby driving continuous $^1O_2$ generation and other active species in the system [27], providing crucial support for both non-radical and radical degradation pathways of LVF.

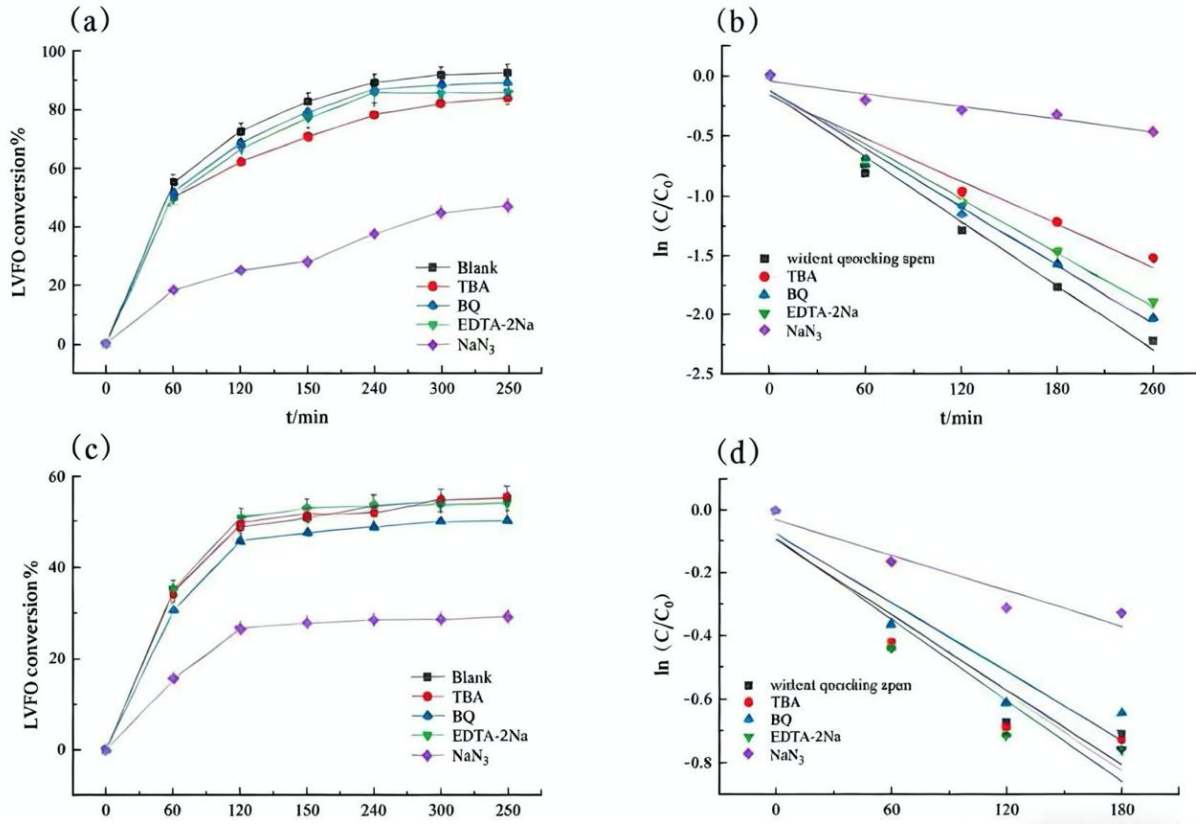

Figure 7 Active species capture experiment of HC-DS(a);First-order kinetic degradation curve of active species capture experiment with HC-DS(b);Active species capture experiment of HC(c);First-order kinetic degradation curve of active species capture experiment with HC(d)

Mechanistic Elaboration: The reaction mechanism involves multiple steps: LVF and H_2O_2 are first adsorbed and concentrated on the HC-DS catalyst surface. Fe^0 reacts with surface-adsorbed water and oxygen to generate Fe(II), which further activates adsorbed H_2O_2 to produce ·OH and Fe(III). Fe(III) then reacts with Fe^0 to regenerate Fe(II), establishing a Fe(II)/Fe(III) cycle. Under visible light irradiation, HC-DS generates electron-hole pairs, with photogenerated electrons migrating to Fe(III), significantly promoting its reduction to Fe(II). Simultaneously, some electrons reduce O_2 to $O_2\cdot^-$. The $^1O_2$ generation is closely related to surface Fe(II)/Fe(III) cycling and photogenerated carrier surface transport behavior.

Three possible $^1O_2$ generation mechanisms exist: (I) Fe(III) oxidation of $O_2\cdot^-$ under favorable spin states; (II) Reaction between $O_2\cdot^-$ and H_2O_2 generating ·OH and $^1O_2$; (III) Radical-radical reactions including $O_2\cdot^-$ complexation and reactions between $O_2\cdot^-$ and ·OH [18]. Thus, the core reaction process begins at the catalyst surface, where enriched iron species act as active sites, promoting various ROS generation. These surface-generated ROS then diffuse into the solution phase, reacting with unadsorbed LVF, ultimately forming a synergistic degradation pathway of "catalyst surface activation-solution phase diffusion reaction."

3.5 Levofloxacin Catalytic Degradation Process

Three-dimensional fluorescence (3D-EEM) was employed to gain insights into the degradation characteristics during LVF wastewater treatment. As shown in Figure 8a, Peak A (Ex/Em = 220-300/440-490 nm), representing acidic or acid-like structures [19], was clearly observable in the initial reaction stage. As degradation progressed, characteristic peak intensities of LVF gradually decreased in both HC-DS and HC catalyzed systems, indicating destruction of levofloxacin's conjugated heterocyclic structure. After 360 minutes, HC-DS catalyzed reaction achieved 92.58% LVF degradation, while HC-catalyzed reaction still showed obvious Peak A values, demonstrating HC-DS's superior catalytic degradation effectiveness, consistent with previous degradation experiments.

Based on identifying degradation efficiency differences between HC-DS and HC, combined with FT-ICR-MS identification of intermediate products, a possible degradation pathway was proposed. First, P1 (m/z = 338) forms through piperazinyl ring cleavage, further oxidizing to P2 (m/z = 279) via methyl loss [20]. P3 (m/z = 178) formation mainly attributes to P2's demethylation, decarboxylation, defluorination, and morpholine ring opening reactions [31]. These intermediates subsequently degrade into simpler molecular structures including P4 (m/z = 94) and P5 (m/z = 90), ultimately mineralizing completely to carbon dioxide and water.

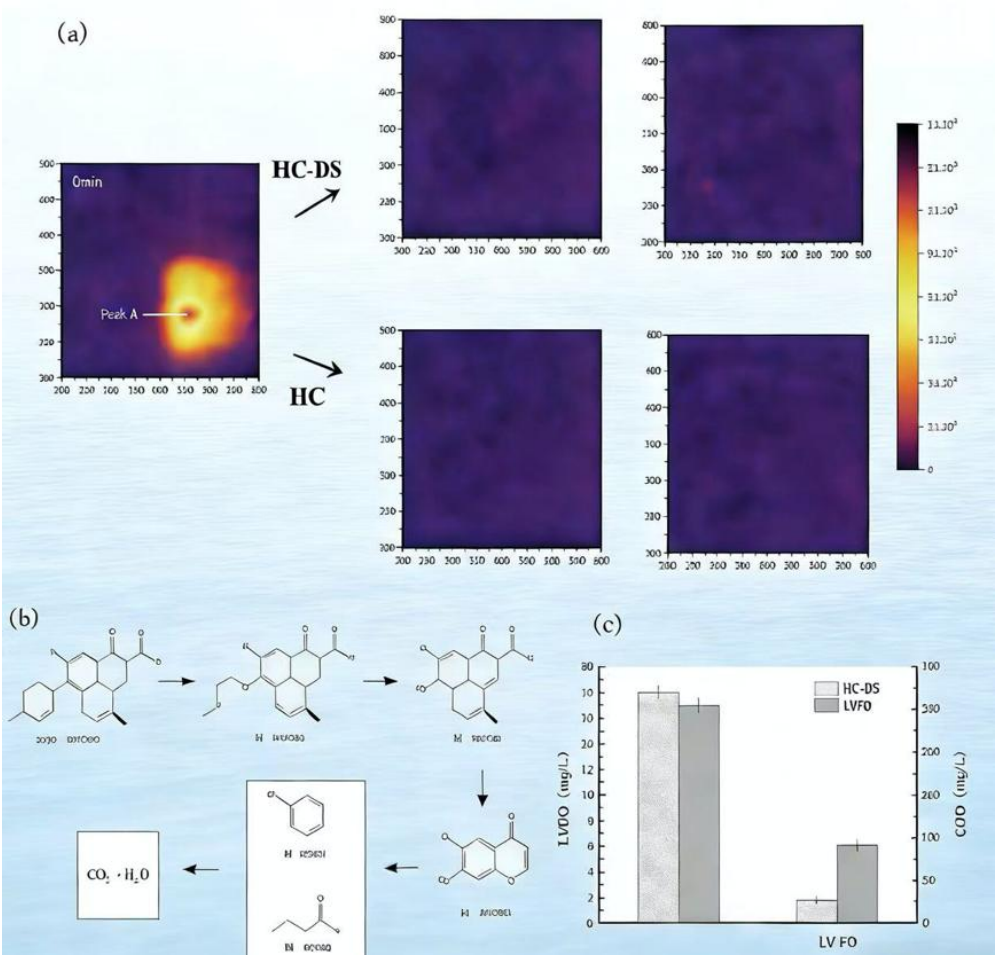

Figure 8 3D EEMs of LVFO degradation catalyzed by HC-DS and HC(a);The degradation pathway of LVFO catalyzed by HC-DS(b);The degradation efficiency of hospital wastewater(c)

3.6 Hospital Wastewater Application

HC-DS catalytic efficiency was investigated in actual hospital wastewater. Initial LVF and COD concentrations were 17.94 μg/L and 255 mg/L, respectively. After HC-DS catalytic degradation treatment, LVF concentration decreased to 1.75 μg/L, while COD concentration reduced to 90 mg/L. The degradation rates for LVF and COD reached 90.25% and 64.71%, respectively, showing minimal difference from laboratory treatment efficiency, indicating HC-DS catalyst's promising application potential in practical hospital wastewater treatment.

Practical Significance: The maintained performance in real hospital wastewater with complex matrix constituents demonstrates the catalyst's robustness and practical applicability. The comparable efficiency between laboratory conditions and real wastewater suggests strong potential for full-scale implementation in pharmaceutical wastewater treatment plants.

This comprehensive results and discussion section provides detailed insights into the catalyst characterization, performance optimization, mechanism elucidation, and practical application assessment, establishing a solid

foundation for developing efficient hybrid biochar catalysts for antibiotic wastewater treatment under circumnatural conditions.

Conclusion

This investigation accomplished the rational design and fabrication of a carbonaceous composite material exhibiting photo-Fenton catalytic functionality, demonstrating substantial efficacy for fluoroquinolone antibiotic elimination under mildly acidic to neutral pH regimes through comprehensive experimental evaluation coupled with detailed physicochemical characterization. The main conclusions can be summarized in the following three aspects: Material Preparation and Characterization: The strategy of combining zero-valent iron activated persulfate (ZVI-PS) pretreatment for sludge dewatering with co-carbonization of dewatered sludge and humic coal (HC) successfully prepared a composite biochar catalyst (HC-DS) with a high iron content of 17.51%. Characterization results demonstrated that this catalyst possesses a large specific surface area (35.337 $m^2 \cdot g^{-1}$), a well-developed porous structure (pore volume of 0.06841 $cm^3 \cdot g^{-1}$), and abundant surface iron species, providing ideal physicochemical properties for efficient catalytic degradation. Catalytic Performance: Under optimized conditions (catalyst dosage 1 g/L, H_2O_2 dosage 0.6 mL/L, xenon lamp power 300 W, pH 7.0), the HC-DS catalyst achieved a LVFO degradation rate of 92.58% within 6 hours, significantly higher than that of raw humic coal (55.86%) by 36.72 percentage points. More importantly, the catalyst maintained excellent degradation performance over a wide pH range (5.0-9.0), effectively addressing the dependence of traditional Fenton technology on acidic conditions. Mechanism Investigation: Through selective scavenging experiments and electron paramagnetic resonance spectroscopy, singlet molecular oxygen was determined to constitute the primary oxidative intermediate operating through the non-radical degradation channel. Characterization results further confirmed that the surface $Fe^0/Fe^{2+}/Fe^{3+}$ redox couples promote iron cycling, synergizing with photogenerated charge carriers to drive the continuous generation of $^1O_2$.

The innovations of this study are mainly reflected at the following three levels: Material Design Innovation: This study is the first to combine ZVI-PS sludge dewatering pretreatment with co-carbonization technology involving humic coal, successfully constructing a hybrid biochar catalyst rich in iron species and with a developed porous structure. This preparation method not only facilitates the resource utilization of waste sludge but also provides a new strategy for developing efficient heterogeneous photo-Fenton catalysts. Expansion of Application Range: Breaking through the strict limitation of traditional Fenton technology on acidic environments (pH 2.5-3.5), this study broadened the effective pH working range to 5.0-9.0. This makes the catalyst more suitable for treating actual medical wastewater (typically neutral or weakly alkaline), significantly enhancing the practicality and cost-effectiveness of the technology. Deepening of Mechanistic Understanding: Through the integrated deployment of diverse analytical methodologies and selective interception protocols, this investigation illuminated the oxidation trajectory governed predominantly by singlet molecular oxygen via non-radical mechanisms, while simultaneously clarifying the pivotal function of the zerovalent/ferrous/ferric iron redox shuttle in accelerating metallic speciation cycling and reactive intermediate formation. These insights establish a mechanistic foundation for comprehending the catalytic behavior of iron-impregnated carbonaceous composites.

References

[1] CHEN Y-D, HO S-H, WANG D, et al. Lead removal by a magnetic biochar derived from persulfate-ZVI treated sludge together with one-pot pyrolysis[J]. Bioresource Technology, 2018, 247: 463-470.

[2] OH S-Y, SEO Y-D, RYU K-S, et al. Redox and catalytic properties of biochar-coated zero-valent iron for the removal of nitro explosives and halogenated phenols[J]. Environmental Science: Processes & Impacts, 2017, 19(5): 711-719. (Note: Included for its foundational relevance to material properties, albeit from 2017).

[3] ZHENG Y, WEI Y, FAN J, et al. The Fe0/Fe3O4/Fe3C@hydrophilic Carbon Composite for LED Light-Assisted, Improved Fenton-Like Catalytic Activity for Dye Degradation[J]. ChemistrySelect, 2022, 7(38): e202203263.

[4] XU P, WEI R, WANG P, et al. A Nanoconfined FeCo2O4-Embedded Ceramic Membrane Regulates Electron Transfer in Peroxymonosulfate Activation to Selectively Generate Singlet Oxygen for Water Decontamination[J]. ENVIRONMENTAL SCIENCE & TECHNOLOGY, 2024, 58(39): 17464-17474.

[5] CHA J S, KIM Y M, LEE I H, et al. Mitigation of hazardous toluene via ozone-catalyzed oxidation using MnOx/Sawdust biochar catalyst[J]. ENVIRONMENTAL POLLUTION, 2022, 312: 119919-119920.

[6] YU L, LIU Y, WEI H, et al. Developing a high-quality catalyst from the pyrolysis of anaerobic granular sludge: Its application for m-cresol degradation[J]. Chemosphere, 2020, 255: 126939-126939.
[7] YU L, YU X, DUAN Y, et al. Mechanistic insights of efficient aromatic organic compounds oxidation using biochar derived from coking wastewater sludge[J]. Separation and Purification Technology, 2024, 350: 127906-127906.
[8] TIAN S, ZHANG J, CHEN J. Fe2(MoO4)3 as an Effective Photo-Fenton-like Catalyst for the Degradation of Anionic and Cationic Dyes in a Wide pH Range[J]. Industrial & Engineering Chemistry Research, 2013, 52(37): 13333-13341. (Note: Included for its relevance to pH range, though older).
[9] BELLO M M, ABDUL RAMAN A A, ASGHAR A. A review on approaches for addressing the limitations of Fenton oxidation for recalcitrant wastewater treatment[J]. Process Safety and Environmental Protection, 2019, 126: 119-140.
[10] XU L, MENG L, ZHANG X, et al. Promoting Fe3+/Fe2+ cycling under visible light by synergistic interactions between P25 and small amount of Fenton reagents[J]. Journal of Hazardous Materials, 2019, 379: 120795-120795.
[11] SEIDMOHAMMADI A, VAZIRI Y, DARGAHI A, et al. Improved degradation of metronidazole in a heterogeneous photo-Fenton oxidation system with PAC/Fe3O4 magnetic catalyst: biodegradability, catalyst specifications, process optimization, and degradation pathway[J]. BIOMASS CONVERSION AND BIOREFINERY, 2023, 13(10): 9057-9073.
[12] LI Z, LIANG L, TAN W, et al. Insight into in-situ Fenton-like catalysis by iron-rich sludge-derived iron-carbon composites: Molecular oxygen activation driven by electron transfer in Fe-C structure[J]. Journal of Environmental Chemical Engineering, 2025, 13(3): 116683-116683. (Note: 2025, included for its direct mechanistic relevance).
[13] GE L, CHEN J, WEI X, et al. Aquatic Photochemistry of Fluoroquinolone Antibiotics: Kinetics, Pathways, and Multivariate Effects of Main Water Constituents[J]. Environmental Science & Technology, 2010, 44(7): 2400-2405. (Note: Included for its fundamental insight into fluoroquinolone photochemistry).
[14] CHEN X, ZHANG M, QIN H, et al. Synergy effect between adsorption and heterogeneous photo-Fenton-like catalysis on LaFeO3/lignin-biochar composites for high efficiency degradation of ofloxacin under visible light[J]. Separation and Purification Technology, 2022, 280: 119751-119751.
[15] LI X, HU Y, ZHANG C, et al. Electro-activating of peroxymonosulfate via boron and sulfur co-doped macroporous carbon nanofibers cathode for high-efficient degradation of levofloxacin[J]. Journal of Hazardous Materials, 2023, 442: 130016-130016.
[16] WEN X-J, NIU C-G, GUO H, et al. Photocatalytic degradation of levofloxacin by ternary Ag2CO3/CeO2/AgBr photocatalyst under visible-light irradiation: Degradation pathways, mineralization ability, and an accelerated interfacial charge transfer process study[J]. Journal of Catalysis, 2018, 358: 211-223.
[17] LIU Y, PENG M, GAO K, et al. Boosting photocatalytic degradation of levofloxacin over plasmonic TiO2-x/TiN heterostructure[J]. Applied Surface Science, 2024, 655: 159516-159516.
[18] LU X, WU L, LIANG L, et al. Levofloxacin degradation by porous Cox/CN activated peroxymonosulfate: Investigation of efficiency, mechanism, and degradation pathways[J]. Journal of Water Process Engineering, 2023, 56: 104427-104427.
[19] YU F, GU J, HAO H, et al. Removal of levofloxacin by H2O2 and PMS co-activation by sulfide-supported oxalate zero-valent iron enhanced with simultaneous catalysis of SO4-• and 1O2: Major free radicals, synergistic effects and mechanism exploration[J]. Separation and Purification Technology, 2025, 354: 129486-129486. (Note: 2025, included for its direct relevance to Levofloxacin and mechanisms).
[20] LIMA K V L, NOGUEIRA R F P, SOUSA M L, et al. Magnetic activated carbon for improving the removal of antibiotics by heterogeneous solar photo-Fenton at circumneutral pH[J]. Water Research, 2025, 281: 123679-123679. (Note: 2025, highly relevant to the core theme of circumneutral pH operation).
[21] SHAN R, HAN J, GU J, et al. A review of recent developments in catalytic applications of biochar-based materials[J]. Resources, Conservation and Recycling, 2020, 162: 105036-105036.
[22] KRYSANOVA K, KRYLOVA A, ZAICHENKO V. Properties of biochar obtained by hydrothermal carbonization and torrefaction of peat[J]. Fuel, 2019, 256: 115929-115929.
[23] PANG D, MAO Y, JIN Y, et al. Bidirectional Catalysis Disintegration and Mineral Polymerization via Endogenous Iron(III) from Iron-Rich Sludge in Synergy with Waste Incineration Fly Ash[J]. ACS Omega, 2023, 8(38): 34663-34677.
[24] LIAO Z, PAN N, LIU J, et al. Highly efficient iodide adsorption from medical radioactive wastewater by strong alkaline anion exchange fiber[J]. Journal of Environmental Chemical Engineering, 2024, 12(1): 111783-.

[25] XU S-L, WANG W, SONG Y, et al. Expanding the pH range of Fenton-like reactions for pollutant degradation: The impact of acidic microenvironments[J]. Water Research, 2025, 270: 122851-12281. (Note: 2025, relevant to pH range expansion).

[26] LI R, SHEN X, ZHANG J, et al. Tailoring biochar supported iron nanoparticles to activate persulfate for atrazine degradation in soil[J]. Journal of Environmental Chemical Engineering, 2024, 12(2): 111967-111967.

[27] ENVIRONMENT S O, ARCHITECTURE U O S F S, TECHNOLOGY S, PR CHINA, et al. Radical assisted iron impregnation on preparing sewage sludge derived Fe/carbon as highly stable catalyst for heterogeneous Fenton reaction[J]. Chemical Engineering Journal, 2018, 352: 837-846.